Single-crystal structure of $HoBaCo_4O_7$ at ambient conditions, at low temperature, and at high pressure

Erick A. Juarez-Arellano,* Alexandra Friedrich, Dan J. Wilson, Leonore Wiehl, Wolfgang Morgenroth, and Björn Winkler
Institut für Geowissenschaften, Goethe-Universität Frankfurt, Altenhöferallee 1, 60438 Frankfurt a.M., Germany

Maxim Avdeev
Bragg Institute, ANSTO, PMB 1, Menai, New South Wales 2234, Australia

René B. Macquart and Chris D. Ling†
School of Chemistry, The University of Sydney, Sydney, New South Wales 2006, Australia
(Received 11 September 2008; revised manuscript received 13 January 2009; published 18 February 2009)

We show that the correct space group of $HoBaCo_4O_7$ at ambient conditions is $P6_3mc$ and that no temperature-induced or pressure-induced structural phase transition occurs down to 100 K or up to 9 GPa. The compressibility of $HoBaCo_4O_7$ is mainly determined by a combination of bond compression and changes in the three-membered and six-membered rings of the kagomé layers. $HoBaCo_4O_7$ is more compressible than structurally related compounds due to the comparatively compressible Co-O bonds. The structural analysis allows us to propose an atomistic model for the extremely high oxygen incorporation capability of $HoBaCo_4O_7$.

DOI: 10.1103/PhysRevB.79.064109 PACS number(s): 61.05.cp, 07.35.+k, 61.66.Fn, 62.50.−p

I. INTRODUCTION

In recent years, a new family of isostructural cobaltates ($MBaCo_{4-x}R_xO_7$, with M=In, Y, Ln and R=Co, Fe, Zn) has been synthesized.[1–3] These cobaltates belong to a new class of geometrically frustrated magnets which not only exhibit interesting magnetic, electronic, thermoelectric, and electrochemical properties but also have a remarkable low-temperature oxygen absorption/desorption capability which makes them suitable as oxygen sensors, oxygen permeation membranes, and solid oxide fuel cells.[4–6]

Karppinen *et al.*[4] showed that $YBaCo_4O_{7+\delta}$ reversibly absorbs and desorbs oxygen up to $\delta \approx 1.5$ within the 470–673 K temperature range. This implies that an amount of oxygen corresponding to ~20% of the total oxygen content is readily loaded or removed by just a relatively minor change in temperature or atmosphere. This oxygen incorporation capability substantially exceeds, in its overall magnitude and in the response sensitivity, the capability found in other systems, e.g., $SrFeO_3$ (perovskite structure) or $YBa_2Cu_3O_7$ (perovskitelike structure).[5,7] Tsipis *et al.*[8] showed that the oxygen hyperstoichiometry is closely related to the mixed-valence states of the cobalt atoms.

It is well known that the oxygen diffusion properties of perovskitelike compounds are affected not only by the temperature and surrounding oxygen partial pressure but also significantly depend on structural details. Therefore, different crystal structures will result in different oxygen diffusion properties. There is currently a discussion in the literature about whether the family $MBaCo_4O_7$ crystallizes in space group $P6_3mc$ or in one of its trigonal subgroups, $P31c$, at ambient temperature; or whether $MBaCo_4O_7$ undergoes a temperature-induced structural phase transition at low temperature.

The designation of the correct space group at ambient temperature in this family is not straightforward because the $MBaCo_4O_{7+\delta}$ crystal structure may depend on the oxygen content. Valkeapää *et al.*[9] identified the unit cell of the oxygen hyperstoichiometric phase $YBaCo_4O_{8.2}$ as a=10.875 Å, b=10.168 Å, and c=12.788 Å, with space group $Pnna$ (based on powder XRD in O_2 atmosphere) while Chmaissem *et al.*[10] reported the crystal structure of $YBaCo_4O_{8.1}$ as having the space group $Pbc2_1$ with a=12.790 Å, b=10.845 Å, and c=10.149 Å (x-ray and neutron powder diffraction).

The variation in the oxygen content could also be responsible for the discrepancies related to the reported temperature dependence of $MBaCo_4O_{7+\delta}$. For example, while Soda *et al.*[11] reported two phase transitions for $YBaCo_4O_{7+\delta}$ at ~105 K and ~70 K [$P6_3mc \rightarrow Pmc2_1 \rightarrow$ unknown, δ=0.15(10), and single-crystal neutron diffraction], Chapon *et al.*[12] reported a phase transition at ~313 K [$P31c \rightarrow Pbn2_1$, δ=−0.05(5), and powder neutron diffraction] but none at low temperatures down to 10 K, and Valldor and Andersson[2] reported a stable phase down to 10 K [$P6_3mc$, δ=unknown, and powder neutron diffraction]. Similarly, for $YbBaCo_4O_{7+\delta}$ Nakayama *et al.*[13] reported a phase transition at ~180 K [$P6_3mc \rightarrow Cmc2_1$, δ=0(1), and powder x-ray diffraction], while Huq *et al.*[6] reported a phase transition at ~175 K in a sample treated under a nitrogen atmosphere [$P31c \rightarrow Pbn2_1$, δ=−0.05(5), and powder x-ray and neutron diffraction]. Huq *et al.*[6] also mentioned that the as-made sample contained two phases. They suggested that one phase (phase A) was oxygen stoichiometric and that the other was oxygen hyperstoichiometric [phase B with δ=0.19(3)]. They reported a phase transition in phase A and none in phase B down to 10 K. For $YBaCo_4O_{8.1}$, Chmaissem *et al.*[10] reported a stable phase down to 10 K. These discrepancies illustrate that the oxygen content, the crystal structure, and the occurrence of structural transitions are intrinsically correlated in this complex system.

Independent of the space group used ($P6_3mc$ or $P31c$), at ambient temperature the $MBaCo_4O_7$ crystal structure contains star-shaped [$O^{[4]}(CoO_3^{[2]})_4$] building blocks [Fig. 1(a)], where the central tetrahedrally coordinated $O^{[4]}$ atom (crys-

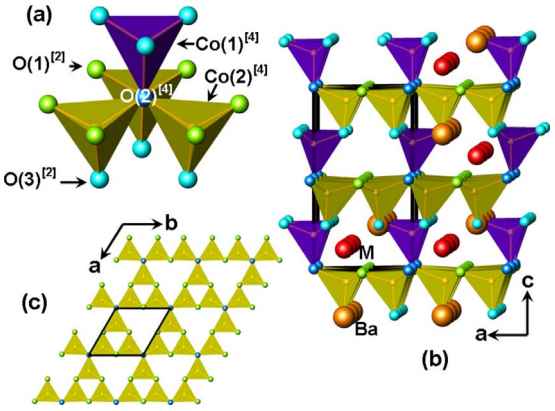

FIG. 1. (Color online) (a) Starlike units. The labels represent the crystallographic sites, while the superscripts represent the coordination numbers. (b) $M\mathrm{BaCo_4O_7}$ crystal structure. (c) kagomé layers. The relative sizes and colors of the atoms were chosen to optimize the visualization.

tallographic $X^{[4]}$ site) simultaneously participates in the coordination of four Co atoms (superscripts denote the number of nearest neighbors). These building blocks are interconnected, thereby forming stable three-dimensional networks. The M and Ba cations, which are found in octahedral and anticuboctahedral coordinations, respectively, occupy channels in the structure formed by $\mathrm{Co_6O_6}$ rings [Fig. 1(b)]. Corner-sharing oxygen tetrahedra form kagomé layers along (001) [Fig. 1(c)].[2]

Due to these structural characteristics, the $M\mathrm{BaCo_4O_7}$ compounds can be viewed as part of the structural family $M_{2-x}A_xR_4W_7$, with $M=(\mathrm{In,Y,Ln})$, $A=(\mathrm{Ba,Ca,Sr,Eu})$, $R=(\mathrm{Si,Al,Co,Fe,Zn})$, and $W=(\mathrm{C,N,O})$. The crystallographic $X^{[4]}$ site is fully occupied by nitrogen in siliconitrides ($M\mathrm{Si_4N_7}$) and aluminiumsiliconoxonitrides ($M\mathrm{Si_{4-x}Al_xO_xN_{7-x}}$) and by carbon in siliconcarbidenitrides ($M_2\mathrm{Si_4N_6C}$). We have already performed high-pressure x-ray diffraction experiments on siliconitrides, aluminiumsiliconoxonitrides, and siliconcarbidenitrides, where no fourfold-coordinated oxygen ions ($O^{[4]}$) have been observed.[14,15] These compounds are very stable with respect to pressure, and no structural phase transition has been observed up to 42 GPa. Nothing is known about the influence of pressure on $M\mathrm{BaCo_4O_7}$ structures, but the apparent thermal instability suggests that these compounds may undergo structural phase transitions at elevated pressures.

In this paper, we have performed an x-ray single-crystal structure determination of $\mathrm{HoBaCo_4O_7}$ at ambient conditions in order to contribute to the discussion about the correct space group. Further measurements were performed at 100 K and at high pressure (up to 9 GPa), searching for temperature-induced and pressure-induced structural phase transitions. We have determined the effect of $O^{[4]}$ links on the compressibility of this compound and compared it with the compressibilities of those silicates already investigated that exhibit $N^{[4]}$ or $C^{[4]}$ links. These findings have thus been used to develop an atomistic model for the mechanism of oxygen uptake, which is a prerequisite for future crystal engineering.

II. EXPERIMENTAL

A. Sample

$\mathrm{HoBaCo_4O_7}$ single crystals were grown from a stoichiometric melt following the procedure described by Bychkov *et al.*[16] The precursors were calcined to ensure dryness and purity. $\mathrm{Ho_2O_3}$ (Sigma-Aldrich, 99.9%) was heated at 1273 K for 15 h, while both $\mathrm{BaCO_3}$ (Merck, 99%) and $\mathrm{Co_3O_4}$ (Sigma-Aldrich, 99.995%) were heated at 873 K for 15 h. Stoichiometric ratios of the precursors were then mixed under acetone in an agate mortar. Upon evaporation of the acetone, the mixture was placed in an alumina crucible covered loosely with an alumina lid, and the whole ensemble was then placed in a second larger crucible. This was done to limit the escape of cobalt and $\mathrm{HoBaCo_4O_7}$ into the furnace at high temperatures. The mixture was heated at a rate of 900 K/h up to 1323 K where it was held for 12 h and then heated at 900 K/h up to 1573 K where it remained for 4 h. The mixture was then cooled at a rate of 1K/h down to 1393 K and then cooled more rapidly to room temperature by switching off the electric power. The quick heating resulted in a melt, from which single crystals were formed during cooling. Black crystals with metallic luster were removed mechanically from the frozen melt by breaking the crucible with a hammer and then using a water-cooled diamond saw to cut away the surrounding noncrystalline matrix. The recovered crystals were washed with water and acetone.

Sample composition was determined by energy dispersive spectroscopy using a FEI Quanta 200 3D scanning electron microscope system equipped with an energy dispersive x-ray analysis (EDAX) Genesis 4000 superultrathin window of energy dispersive x-ray spectroscopy (EDS) microanalysis system. A typical crystal had a cation ratio of $\mathrm{Ho_{1.14}BaCo_{3.93}}$ normalized to the Ba content. The measurements were carried out against standards, so the intrinsic error is less than 10%.

Thermogravimetric analysis (TGA) was performed using a Setaram SetSys 16/18 instrument. The oxygen content was found to have a stoichiometric value, $\delta=0.0(1)$. The results of the detailed comparative study of the behavior of powder and single-crystal samples of $M\mathrm{BaCo_4O_{7+\delta}}$ materials as a function of partial oxygen pressure and temperature will be published elsewhere.

B. X-ray diffraction at ambient conditions and at 100 K

Single-crystal x-ray diffraction data were collected at 100 K and at ambient conditions, using an Xcalibur3 κ-circle diffractometer from Oxford diffraction with a charge coupled device (CCD) camera and Mo K_α radiation from a Mo anode operating at 50 kV and 40 mA. Our Xcalibur3 instrument is equipped with a cryostream system (cryojet HT Oxford diffraction). This allows us to maintain the sample temperature within ± 2 K throughout the measurement. A black metallic single crystal of $120\times105\times75$ $\mu\mathrm{m}^3$ was used, mounted at a distance of 4.2 cm from the detector. We collected 969 frames with a frame width of 0.75° and exposure time of 105 s. Data reduction and absorption corrections using trigonal Laue symmetry for corrections were performed using the program CRYSALIS.[17] The starting atomic positions were ob-

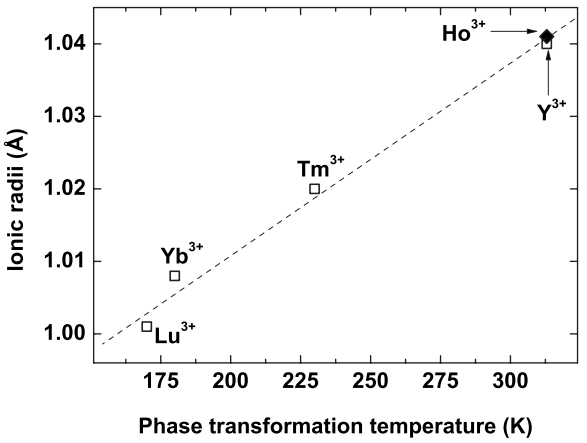

FIG. 2. Correlation between the reported transition temperature of some $MBaCo_4O_7$ family members and the ionic radii (Ref. 28) of the trivalent cations Lu and Tm (Ref. 13) ($P6_3mc \rightarrow Cmc2_1$), Yb (Ref. 6) ($P31c \rightarrow Pbn2_1$), Y (Ref. 29) ($P31c \rightarrow Pbn2_1$), and Ho (inferred). The dashed line is a guide to the eye.

tained by direct methods using SIR-2004 (Ref. 18) and the structure refinements were carried out with SHELXL97-2,[19] using the WINGX (Ref. 20) interface.

C. High-pressure x-ray diffraction

High-pressure single-crystal x-ray diffraction experiments were performed at various pressures up to 9 GPa at HASYLAB (Hamburg, Germany) using the diamond-anvil cell (DAC) technique. A HUBER four-circle diffractometer with Eulerian geometry was used at HASYLAB at the bending-magnet beamline D3 using synchrotron x-ray radiation. A NaI point detector and a wavelength of 0.45 Å, provided by a Si(111) double-crystal monochromator, were used. We employed an ETH-type DAC equipped with beryllium backing plates.[21] A single crystal ($133 \times 107 \times 52$ μm^3) was loaded together with ruby crystals, which were used for pressure determination. A methanol-ethanol (4:1) mixture was used as a pressure-transmitting medium. A hole of 270 μm in diameter, serving as a pressure chamber, was drilled through a steel gasket (preindented to a thickness of 80 μm) using a spark-eroding drilling machine. Before and after each set of measurements, the pressure was determined using the laser-induced ruby-fluorescence technique, applying the pressure scale of Mao *et al.*[22] Full intensity data of $HoBaCo_4O_7$ were collected at 3.0(1), 6.5(3), and 8.8(1) GPa, while the data which were measured solely for the purpose of accurate cell parameter determination were collected at 1.0(1), 4.5(1), and 7.2(1) GPa. The intensity data collection at high pressures was carried out with ω-scans, according to the fixed-ϕ technique,[23] in order to select the beam path of the least attenuation through the pressure cell. Intensity data were obtained from the scan data by the Lehmann-Larsen algorithm implemented in the beamline-specific software REDUCE (Ref. 24) and corrected for Lorentz and polarization effects as well as for intensity drifts of the primary beam [AVSORT (Ref. 25)]. All data were corrected for absorption by the crystal and the DAC components using the program ABSORB version 6.0.[26] Structural refinements were carried out with SHELXL97-2.[19] The starting parameters for the refinements were taken from our data collected at ambient conditions. Pressure-volume data were fitted using a second-order or third-order Birch-Murnaghan equation of state (BM-EOS) using the program EOS-FIT (Ref. 27) and a fully weighted least-squares procedure.

TABLE I. Details of the data collection, crystal data, agreement factors, isotropic, and anisotropic displacement parameters (Å^2) of $HoBaCo_4O_7$ at ambient conditions and at low temperature.

Crystal data[a]			
Space group	$P6_3mc$	$P31c$	$P6_3mc$
T (K)	298	298	100
a (Å)	6.3051(7)	6.3051(7)	6.3001(6)
c (Å)	10.2286(9)	10.2286(9)	10.1979(8)
V (Å^3)	352.15(6)	352.15(6)	350.54(5)
Density (g cm^{-3})	6.130	6.130	6.158
Linear abs. coeff. (mm^{-1})	25.794	25.794	25.913
Data collection[b]			
h	$\bar{8}$; 8	$\bar{8}$; 8	$\bar{8}$; 8
k	$\bar{7}$; 7	$\bar{7}$; 7	$\bar{8}$; 8
l	−14; 14	−14; 14	−14; 14
Observed reflections	2398	2398	3579
Unique reflections	428	682	413
Reflect. $I>2\sigma(I)$	408	652	399
Parameters	33	41	33
R_{int}	0.0365	0.0321	0.0480
R_{sigma}	0.0177	0.0212	0.0185
$R1[I>2\sigma(I)]$	0.0185	0.0265	0.0186
$R1$(all)	0.0198	0.0279	0.0192
$wR2$	0.0490	0.0732	0.0466
S	1.221	1.082	1.168
$\Delta\rho_{max}$	1.26	1.15	0.96
$\Delta\rho_{min}$	−0.87	−1.01	−1.04
Displacement parameters[c]			
Atom	U_{iso}	U_{iso}	U_{iso}
Ho	0.0102(2)	0.0103(2)	0.0085(2)
Ba	0.0198(2)	0.0197(3)	0.0145(2)
Co(1)	0.0109(3)	0.0110(3)	0.0083(3)
Co(2)	0.0102(2)	0.0102(2)	0.0071(2)
O(1)	0.040(2)	0.040(2)	0.043(2)
O(2)	0.016(2)	0.016(2)	0.012(2)
O(3)	0.040(2)	0.041(3)	0.044(3)

[a]Z (formula units)=2; molecular weight=1299.98 g mol^{-1}; F(000)=574 e^-.
[b]Four-circle diffractometer (Xcalibur3, Oxford diffraction), CCD camera, and λ=0.71073 Å.
[c]ADPs can be found at the FIZ-Karlsruhe database under the depository numbers 420423 (P63mc-298 K) and 420424 (P63mc-100 K).

III. RESULTS AND DISCUSSION

A. Crystal structure of $HoBaCo_4O_7$ at ambient conditions

Phase transformations have previously been reported in some of the $MBaCo_4O_7$ family members (M=Lu^{3+}, Yb^{3+}, Tm^{3+}, and Y^{3+}) at different temperatures.[6,12,13] From these reports and considering only compounds with stoichiometric oxygen content, we have correlated the transition temperature with the ionic radii of the trivalent cations (Fig. 2). Following this correlation, we expected the structural behavior of Ho^{3+} [1.041 Å (Ref. 28)] to be similar to the Y^{3+} compound (1.04 Å and Fig. 2). This could imply a transition from $P31c$ (high T phase) to $Pbn2_1$ (low T phase) at 313 K (Ref. 12), and if that transition occurs, the $Pbn2_1$ should be considered as the correct space group at ambient conditions. However, at ambient conditions the structure of $HoBaCo_4O_7$ was reported by Sheptyakov *et al.*[1] and Valldor[3] based on powder x-ray diffraction data in space group $P6_3mc$ with unit-cell parameters, a=6.30 Å, c=10.22 Å, V=350.5 $Å^3$, and Z=2. The main difference between the space group $P6_3mc$ and the subgroup $P31c$ is a mirror plane perpendicular to the a axis. Thus, in order to clarify in which space group $HoBaCo_4O_7$ crystallizes at ambient conditions, the space groups $P6_3mc$, $P31c$, and $Pbn2_1$ were all evaluated.

The starting atomic positions for the space groups $P6_3mc$ and $P31c$ were obtained from our data collected at ambient conditions by direct methods using SIR-2004.[18] However, it was not possible to obtain them for $Pbn2_1$, so instead we used previously reported values.[6] Refinement using the $Pbn2_1$ model always diverged, and therefore this approach was abandoned. In contrast, very similar results were observed for the $P6_3mc$ and $P31c$ models (Table I).

Huq *et al.*[6] justified the $P31c$ symmetry of $YbBaCo_4O_7$ using two criteria: (1) a statistical analysis based on $R_{int}(F^2)$ (13.3% for $P6_3mc$ and 5.5% for $P31c$), where R_{int} is a measure of how well the intensities of symmetry-equivalent reflections correspond to each other[30] and (2) anomalously large isotropic displacement parameters (IDPs) of three atoms [Co(2), O(1), and O(3)] lying on a mirror plane. In our single-crystal results, the $R_{int}(F^2)$ are rather similar in both cases, around 3% (Table I), although refinement conventional indices such as R_1 [based on observed I values larger than $2\sigma(I)$] suggest that the best refinement is obtained with $P6_3mc$ even though the difference is subtle. The agreement factors are shown in Table I. Considering that $P6_3mc$ and $P31c$ have identical extinction conditions ($hh\bar{2}hl$: l=2n+1 and 000l: l=2n+1), it is difficult to say which model is best simply by evaluating the figures of merit. However, comparing the intensities of symmetry-equivalent reflections gives an irrefutable argument. For example, for $P31c$, the reflections ($h0\bar{h}l$), ($\bar{h}h0l$), and ($0\bar{h}hl$) should have equivalent intensities which differ from ($\bar{h}0hl$), ($h\bar{h}0l$), and ($0h\bar{h}l$), while for $P6_3mc$ the six reflections should have equivalent intensities.[31] We compared the intensities of several sets of reflections such as (101), ($\bar{1}11$), ($0\bar{1}1$), ($\bar{1}01$), ($1\bar{1}1$), and (011), or (102), ($\bar{1}12$), ($0\bar{1}2$), ($\bar{1}02$), ($1\bar{1}2$), and (012) and found that all of them have equivalent intensities. It is worthwhile emphasizing that this type of analysis is only possible with single-crystal data. In order to extend this analysis, we used the ADDSYM function within the PLATON software.[32] This software helps to detect additional symmetry elements for a given set of atomic coordinates.[33–35] Running ADDSYM using the $P31c$ model, the program found missing symmetry operations including the screw axis (6_3) and mirror planes. Taking these missed symmetries into consideration, ADDSYM suggested the space group $P6_3mc$ in agreement with our previous findings.

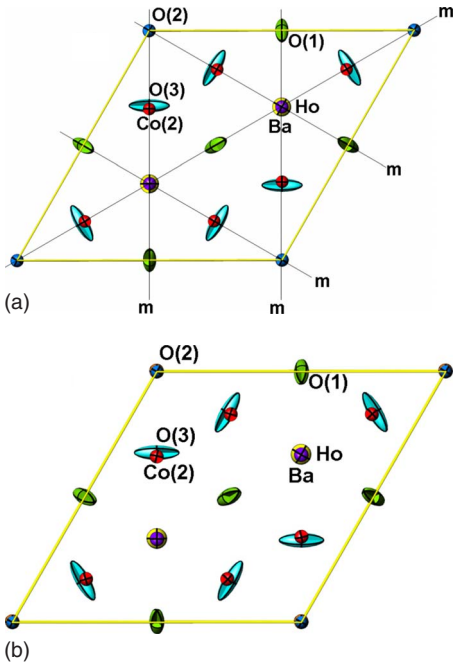

FIG. 3. (Color online) Independent anisotropic displacement parameters (ADPs at 50% probability level) at room conditions. (a) $P6_3mc$ and (b) $P31c$ models, respectively.

Turning to the displacement parameters, refinements carried out with independent anisotropic displacement parameters (ADPs) for all atoms gave no unusual or anomalously large thermal parameters for Co(2). However, we observed slightly elongated O(1) and O(3) thermal ellipsoids irrespective of the chosen space group (Fig. 3). Changing from $P6_3mc$ to $P31c$, the mirror plane on which the Co(2), O(1), and O(3) atoms lie is eliminated. Therefore, if the distortions of the thermal ellipsoids were generated by a split position in the $P6_3mc$ model, they should lead to significant changes in the $P31c$ model. However, the oxygen thermal ellipsoids were nearly the same in both models (Fig. 3 and Table I), and only a subtle change in the Co(2), O(1), and O(3) orientation of the ADPs can be detected in $P31c$ as a result of the lower symmetry.

Looking at the three single-crystal data sets reported to date ($MBaCo_4O_7$, with M=Y, Dy, In),[2,3] we found that the oxygen ADPs were reported only for the yttrium structure and that the same slightly elongated O(1) and O(3) thermal ellipsoids were observed. Furthermore, in the case of $DyBaCo_4O_7$,[3] where only oxygen IDPs were reported, the values of the O(1) and O(3) IDPs were around two times bigger than the O(2) IDP value, which agrees with what we have found in this work (Table I). Additionally, single-crystal

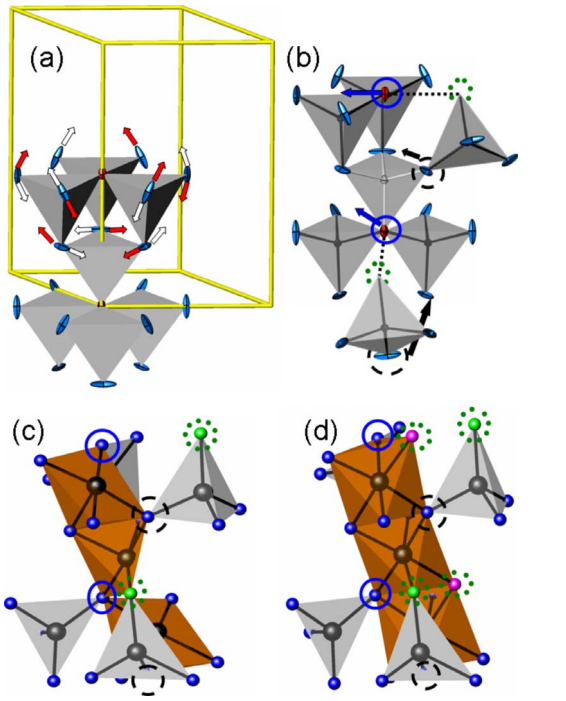

FIG. 4. (Color online) (a) Coupled twist movements of oxygen ADPs (solid and empty arrows). (b) $O^{[4]}$ broken bonds (black dashed line), space generated in order to allow interaction with new oxygen atoms (green dotted circles) and tetrahedra tilting (arrows). The circles (black dashed and blue solid) were chosen to optimize the tilting visualization. (c) The coordination of some of the cobalt polyhedra changed ($Co^{[5]}$). (d) The combination of the $O^{[4]}$ broken bond and the tetrahedra tilting generates space for the interaction of a second new oxygen atom, increasing the cobalt coordination to $Co^{[6]}$ and acquiring the $YBaCo_4O_{8.1}$ structure (Ref. 10).

data sets of 14 isotypic compounds [$LuBaZn_{3.09}Al_{0.91}O_7$, $YBaCo_3FeO_7$, $CaBaZn_2FeAlO_7$, and $CaBaCo_{4-x-y-z}Zn_xFe_yAl_zO_7$ (Refs. 3, 36, and 37)] show the same tread for the IDPs and ADPs. Thus, deformations of the thermal ellipsoids on the oxygen ions are related to the nature of the system and are not an artifact related to an incorrect space-group assignation. Therefore, we consider that, at least for $HoBaCo_4O_7$, the best description of the crystal structure at ambient conditions is obtained with the space group $P6_3mc$.

Examining the oxygen ADPs in $HoBaCo_4O_7$, which are characteristic of this isotypic family, we can identify a coupled twist movement of the tetrahedral network [Fig. 4(a)] with the fourfold coordinated O(2) [$O^{[4]}$, Fig. 1(a)] as center around which the rotation occurs. It is not difficult to see, then, that when the temperature is increased, the coupled twist movement will increase due to the thermal motion. If there is an oxygen-rich environment, it will be easy for a new oxygen atom to interact with the tetrahedral network. This interaction will be enhanced by the Co^{3+} ions, which prefer octahedral coordination. Considering that the $P6_3mc$ model does not have available sites for extra oxygen, the crystal structure has to change in order to promote this interaction. The most logical place for this change is the $O^{[4]}$ site, where one of the $O^{[4]}$ bonds can be broken, creating space for the interaction with the new oxygen atom [Fig. 4(b)]. Consequently, the old $O^{[4]}$ site [O(1)] is transformed into two sites $O^{[3]}$[O(1)′] and $O^{[2]}$[O(new)]. The new configuration produces tetrahedral tilting, increasing the coordination of some of the cobalt polyhedra ($Co^{[5]}$) [Fig. 4(c)]. The combination of the $O^{[4]}$ broken bond and the tetrahedral tilting creates space for the interaction of a second new oxygen atom, increasing once more the coordination of some of the

TABLE II. Details of the data collection, crystal data, agreement factors, isotropic, and anisotropic displacement parameters (Å^2) of $HoBaCo_4O_7$ at pressures up to 9 GPa. Space group $P6_3mc$.

Crystal data[a]			
p/GPa	3.0(1)	6.5(3)	8.8(1)
a (Å)	6.256(5)	6.206(4)	6.168(5)
c (Å)	10.142(6)	10.040(4)	9.976(5)
V (Å^3)	343.8(5)	334.9(3)	328.6(4)
Density (g cm^{-3})	6.279	6.446	6.569
Linear abs. coeff. (mm^{-1})	7.64	7.84	7.99
Data collection[b]			
h	$\bar{5}$; 5	$\bar{4}$; 4	$\bar{5}$; 5
k	$\bar{8}$; 8	$\bar{7}$; 7	$\bar{8}$; 7
l	−14; 14	−12;11	−13; 12
Observed reflections	1264	861	1096
Unique reflections	370	269	353
Reflect. $I>2\sigma(I)$	360	260	337
Parameters	33	33	33
R_{int}	0.0856	0.0479	0.0523
R_{sigma}	0.0419	0.0287	0.0363
$R1[I>2\sigma(I)]$	0.0514	0.0277	0.0267
$R1$(all)	0.0391	0.0304	0.0292
$wR2$	0.0927	0.0638	0.0570
S	1.319	1.238	1.195
$\Delta\rho_{max}$	1.24	0.80	0.85
$\Delta\rho_{min}$	−1.14	−0.84	−0.97
Displacement parameters[c]			
Atom	U_{iso}	U_{iso}	U_{iso}
Ho	0.0100(3)	0.0106(3)	0.0112(2)
Ba	0.0202(4)	0.0226(4)	0.0244(3)
Co(1)	0.0113(5)	0.0126(5)	0.0120(4)
Co(2)	0.0106(4)	0.0118(4)	0.0118(3)
O(1)	0.048(4)	0.057(5)	0.066(5)
O(2)	0.012(3)	0.010(3)	0.011(3)
O(3)	0.044(5)	0.053(5)	0.053(5)

[a]The data collection was performed at ambient temperature.
[b]Four-circle diffractometer (HUBER, D3, HASYLAB), point detector, λ=0.45 Å, ω scan (step-scan mode with 71 steps), $\Delta\omega$=0.02°, and standards: (0.6.6) and (1.1.14).
[c]ADPs can be found at the FIZ-Karlsruhe database under the depository numbers 420425 (P63mc-3 GPa), 420426 (P63mc-6.5 GPa) and 420427 (P63mc-8.8 GPa).

TABLE III. Atom positions of $HoBaCo_4O_7$ from the experiment at 100 K, ambient conditions, and as a function of pressure.

p/GPa	Wyckoff position	0.0001	0.0001	3.0(1)	6.5(3)	8.8(1)
T (K)		100	298	298	298	298
Ho, z [a]	2*b*	0.9998(1)	0.9997(1)	0.9988(1)	0.9998(1)	0.9998(1)
Ba, z [a]	2*b*	0.6273(1)	0.6271(1)	0.6256(2)	0.6260(1)	0.6259(1)
Co(1), z [b]	2*a*	0.5671(3)	0.5670(2)	0.5653(5)	0.5650(5)	0.5640(4)
Co(2), x [c]	6*c*	0.1708(1)	0.1706(1)	0.1711(1)	0.1716(1)	0.1720(1)
Co(2), z		0.8146(2)	0.8138(2)	0.8126(3)	0.8132(3)	0.8120(2)
O(1), x [c]	6*c*	0.4999(7)	0.4995(5)	0.500(1)	0.500(1)	0.501(1)
O(1), z		0.8772(8)	0.8765(7)	0.875(2)	0.875(2)	0.874(1)
O(2), z [b]	2*a*	0.3831(9)	0.3803(7)	0.380(2)	0.380(2)	0.377(1)
O(3), x [c]	6*c*	0.8380(6)	0.8376(5)	0.839(1)	0.836(1)	0.837(1)
O(3), z		0.1258(5)	0.1263(4)	0.123(1)	0.126(1)	0.125(1)

[a] $x=\frac{2}{3}; y=\frac{1}{3}$.
[b] $x=y=0$.
[c] $y=-x$.

cobalt polyhedra ($Co^{[6]}$), thus leading to the oxygen hyperstoichiometric structure reported by Chmaissem *et al.*[10] ($YBaCo_4O_{8.1}$) [Fig. 4(d)]. Following the ideas above and considering that in the $YBaCo_4O_{8.1}$ structure not all the $O^{[4]}$ had changed, we think that as long as untwisted $O^{[4]}$ remains in the structure there is a possibility of absorbing more oxygen, as was reported by Tsipis *et al.*[7] ($YBaCo_4O_{8.58}$), Hao *et al.*[38] ($ErBaCo_4O_{8.61}$), and Karppinen *et al.*[4] ($YBaCo_4O_{8.5}$). Therefore, we conclude that the oxygen in fourfold coordination ($O^{[4]}$) is the key to the absorption mechanism of this type of compound.

B. Crystal structure of $HoBaCo_4O_7$ at low temperature

A careful search for split reflections, which could indicate a low-symmetry structure, was performed without success in the data set collected at 100 K. Therefore, no temperature-induced structural phase-transition breaking the threefold symmetry was detected down to 100 K. The $P31c$ model was also tested, and the ADDSYM program was used, with the same result as for ambient conditions. The agreement factors, the isotropic, and anisotropic displacement parameters of $HoBaCo_4O_7$ at ~100 K are summarized in Table I.

Comparing the cation's IDP values at ambient temperature and at 100 K (Table I), we observe the reduction in the thermal motion of most of the IDP values, but we also observe a sharpening of the elongation of the thermal ellipsoids of O(1) and O(3), which is an indication of static disorder. This disorder could be related to variations in the oxygen's atomic positions between unit cells[30] or to structural defects (e.g., dislocations and stacking faults[39]).

C. Crystal structure of $HoBaCo_4O_7$ at high pressure

The pressure dependence of the unit-cell parameters, details of the data collection, agreement factors, IDPs, and ADPs of $HoBaCo_4O_7$ up to 9 GPa are summarized in Table II. Atomic positions and interatomic distances and angles are shown in Tables III and IV, respectively. No evidence for a pressure-induced structural phase transformation was observed up to 9 GPa.

1. Bulk compressibility

The variation in the normalized unit-cell volume and lattice parameters as a function of pressure is plotted in Fig. 5. Results of fits of second-order or third-order BM-EOS to the pressure-volume data and the pressure dependencies of the individual cell axes are summarized in Table V.

Although similar values were obtained for the bulk moduli from the second-order and third-order BM-EOS fittings, a considerable deviation in the values of the first pressure derivative was observed. In order to identify the most appropriate order of the BM-EOS, the p-V data were transformed into normalized stress (F) and Eulerian strain (f), respectively (Fig. 6). For a BM-EOS (Ref. 40) the Eulerian strain is given by $f=1/2[(V_0/V)^{2/3}-1]$ and the normalized stress is defined as $F=p[3f(1+2f)^{5/2}]^{-1}$. If the data points lie on a horizontal line, with constant F, then the data can be fitted with a second-order BM-EOS ($B'=4$). If the data points lie on an inclined straight line, the data will be adequately described by a third-order BM-EOS. Positive or negative slope implies $B'>4$ and $B'<4$, respectively. In all cases, the value of the intercept on the F axis is equal to the B_0 value.[40] The negative slope in the F-f plot (Fig. 6) indicates that the pressure derivative of the bulk modulus is smaller than 4. For a better visualization, F-f values using the results of the second-order and third-order BM-EOS fits were calculated using the program EOS-FIT (Ref. 27) and plotted in Fig. 6.

The value of the first derivative of the bulk modulus using a third-order BM-EOS ($B'=1.5$) appears unusual at first glance, as for solids where the compression is controlled by central forces between atoms, the B' value is between 3.8 and 8.[40,41] However, this constraint is not applicable to structures which compression behavior is dominated by polyhe-

TABLE IV. Interatomic distances (Å) and angles (°) of $HoBaCo_4O_7$ from the experimental data.

p/GPa	0.0001	0.0001	3.0(1)	6.5(3)	8.8(1)
T (K)	100	298	298	298	298
Ho-O(1) (3x)	2.207(7)	2.218(5)	2.20(1)	2.18(1)	2.17(1)
-O(3) (3x)	2.269(6)	2.271(5)	2.25(1)	2.22(1)	2.21(1)
⟨Ho-O⟩	2.238(7)	2.245(5)	2.23(1)	2.20(1)	2.19(1)
Ba-O(1) (3x)	3.132(9)	3.137(7)	3.11(2)	3.08(2)	3.04(2)
-O(1)′ (3x)	3.132(9)	3.140(7)	3.12(2)	3.09(2)	3.09(2)
-O(3x) (6x)	3.151(1)	3.153(1)	3.13(1)	3.10(1)	3.08(2)
⟨Ba-O⟩	3.142(5)	3.146(4)	3.12(2)	3.09(2)	3.07(2)
Co(1)-O(2) (1x)	1.877(10)	1.910(8)	1.88(2)	1.86(1)	1.86(1)
-O(3) (3x)	1.867(6)	1.874(5)	1.85(1)	1.86(1)	1.85(1)
⟨Co(1)-O⟩	1.870(7)	1.883(6)	1.86(1)	1.86(1)	1.85(1)
Co(2)-O(1) (2x)	1.906(4)	1.908(3)	1.90(1)	1.87(1)	1.87(1)
-O(2) (1x)	1.990(3)	1.983(3)	1.97(1)	1.96(1)	1.95(1)
-O(3) (1x)	1.928(6)	1.920(5)	1.92(1)	1.88(1)	1.87(1)
⟨Co(2)-O⟩	1.933(4)	1.930(4)	1.92(1)	1.89(1)	1.89(1)
O(1)-Ho-O(1)′ (3x)	91.1(3)	90.9(3)	90.6(7)	90.4(6)	89.8(6)
O(1)-Ho-O(3) (6x)	88.9(2)	89.2(2)	88.9(4)	89.4(4)	89.6(3)
O(1)′-Ho-O(3) (3x)	179.9(3)	179.9(2)	179.2(5)	179.8(5)	179.1(5)
O(3)-Ho-O(3)′ (3x)	91.0(2)	90.7(1)	91.7(4)	90.8(4)	91.0(4)
O(3)-Co(1)-O(3)′ (3x)	110.2(2)	110.1(1)	110.4(3)	109.8(4)	109.6(3)
O(3)-Co(1)-O(2) (3x)	108.7(2)	108.9(1)	108.5(3)	109.1(4)	109.3(3)
O(1)-Co(2)-O(1)′ (1x)	111.4(5)	111.0(4)	111.6(9)	112.1(9)	112.9(8)
O(1)-Co(2)-O(3) (2x)	110.9(3)	110.9(2)	111.0(6)	110.6(5)	110.7(5)
O(1)-Co(2)-O(2) (2x)	107.9(2)	108.3(2)	108.0(4)	108.0(3)	107.8(3)
O(3)-Co(2)-O(2) (1x)	107.7(3)	107.4(3)	107.1(5)	107.3(5)	106.6(5)

dron tiltings.[40] Hofmeister and Mao[42] showed that values of B' below 4 lead to unstable structures at sufficiently high compression, where the structure collapses. Recently, we have performed *in situ* high-pressure synchrotron x-ray powder-diffraction experiments on different members of the $MBaCo_4O_7$ family and obtained comparable B' values to those in this study. Moreover, in those experiments we observed that the structure collapses at pressures above 10 GPa (becoming amorphous). These results will be published elsewhere. Therefore, we consider that the third-order BM-EOS yields an adequate representation of the data set and that the small value of B' probably is an indication of the structural instability at pressures higher than those investigated here.

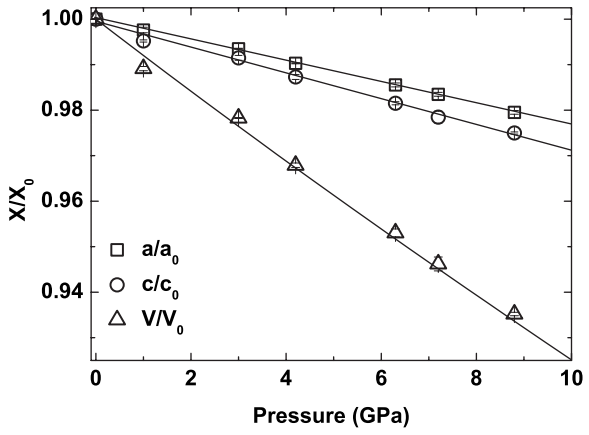

FIG. 5. Normalized unit-cell volume and lattice parameters as a function of pressure for $HoBaCo_4O_7$ up to 9 GPa. BM-EOS fits to the data are represented by lines.

It has been proposed that for isostructural compounds the product of the molar volume and the bulk modulus should be constant [B_0V_0=const (Ref. 43)]. For those structurally related compounds for which the compressibility is known [$SrYbSi_4N_7$ [B_0=176(2) GPa, V_0=302.91(6) Å^3], and $MYbSi_{4-x}Al_xO_xN_{7-x}$, M=Sr[161(2), 310.4(1)] and Ba[168(2), 317.3(5)], and x=2 (Ref. 14)] that holds, B_0V_0 =52197(±2.1%). However, for $HoBaCo_4O_7$ the B_0V_0 ≃43296 and hence is significantly lower than expected.

Generally, the properties of a compound depend on a combination of different factors such as the crystal structure, the type of atoms and the nature of the bonds between them. Thus, in structurally related compounds, the difference in compressibilities is mainly related to the type of atoms and the nature of the bonds between them. Moreover, it is known that the tetrahedral network dominates the compressibility in siliconitrides, aluminiumsiliconoxonitrides, and siliconcarbidenitrides.[14,15,44] Therefore, we will focus our discussion on the corner-sharing tetrahedral network [star-shaped building blocks, $X^{[4]}(RW_3^{[2]})_4$; (X,W)=N,C,O and

TABLE V. Bulk modulus, linear compressibility, and polyhedra compression results from fits of Birch-Murnaghan equations of state to the experimental data of $HoBaCo_4O_7$.

V_0 (Å^3)	B_0 (GPa)	B'
352.2(2)	113(3)	4 (fixed)
352.2(2)	123(2)	1.5(2)
a_0 (Å)	K_{a_0} (GPa)	
6.3051(7)	118(4)	4 (fixed)
c_0 (Å)	K_{c_0} (GPa)	
10.2286(8)	100(3)	4 (fixed)
Ho-O_{V_0} [a] (Å^3)	O_{B_0} [b] (GPa)	
14.98(3)	107(6)	4 (fixed)
Co(1)-T_{V_0} (Å^3)	T_{B_0} (GPa)	
3.45(2)	108(32)	4 (fixed)
Co(2)-T_{V_0} (Å^3)	T_{B_0} (GPa)	
3.70(1)	108(7)	4 (fixed)

[a] O_{V0} and T_{V0} represent the octahedra and tetrahedra volumes, respectively.

[b] O_{B0} and T_{B0} represent the octahedra and tetrahedra bulk moduli.

R=Si,Al,Co]. A comparison of $R-X^{[4]}$ and $R-W^{[2]}$ bond lengths is shown in Fig. 7.

In contrast to structurally related compounds, where the $R-X^{[4]}$ bond lengths are significantly longer than $R-W^{[2]}$ (Fig. 7), in $HoBaCo_4O_7$ the $R-X^{[4]}$ [Co-O(2)] and $R-W^{[2]}$ [Co-O(1) and -O(3)] bond lengths have similar magnitudes. Therefore, the larger Co-O bond lengths (Fig. 7) make $HoBaCo_4O_7$ more compressible than structurally related siliconitrides, aluminiumsiliconoxonitrides, or siliconcarbidenitrides.

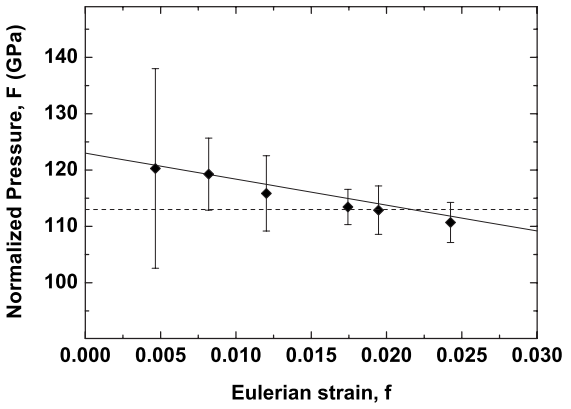

FIG. 6. Pressure-volume data plotted as normalized stress (F) against Eulerian strain (f). Calculated F-f values using B_0 =113 GPa, B'=4 and B_0=123 GPa, B'=1.5 are plotted as dashed and solid lines, respectively.

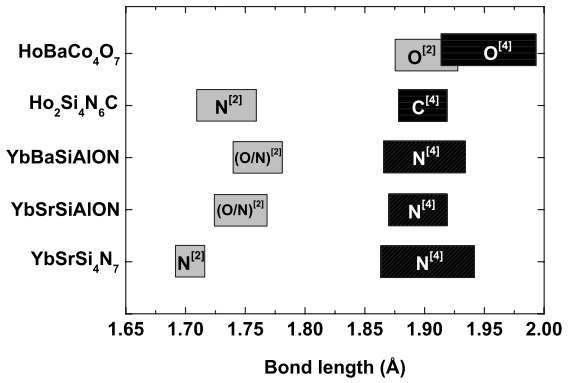

FIG. 7. Comparison of bond lengths of structurally related compounds [$R-X^{[4]}$ and $R-W^{[2]}$, R=Si,(Si/Al),Co; and (X,W) =N,C,O]. From top to bottom: $HoBaCo_4O_7$ (this work), $Ho_2Si_4N_6C$ (Ref. 45), MYbSi$_{4-x}$Al$_x$O$_x$N$_{7-x}$ (M=Ba,Sr) (Ref. 46), and $YbSrSi_4N_7$ (Ref. 47). Superscripts represent the coordination number.

To analyze the polyhedron compressions, the volumes of the HoO_6, $Co(1)O_4$, and $Co(2)O_4$ polyhedra were calculated using the program VOLCAL (Ref. 48) (Table V). The normalized polyhedron volumes, as a function of pressure, are plotted in Fig. 8 which shows that the compressibility of all polyhedra is similar.

2. Linear compressibility

The pressure dependence of the unit-cell parameters shows that, even though the a and c axes behave similarly on compression, the c axis is more compressible (Fig. 5 and Table V). This trend is increased upon pressure increase. In isotypic compounds the same trend is observed although in YbBaSi$_{4-x}$Al$_x$O$_x$N$_{7-x}$ the compression of a and c is almost equal up to the highest pressure achieved (37 GPa). In $M_2Si_4N_6C$ (M=Ho,E; $P12_1/c1$) the monoclinic lattice parameters are related to the hexagonal lattice as $a_m \sim a_h$, $c_m \sim 2b_h$, $b_m \sim c_h$, and $\beta \sim 120°$, with b_m being the most compressible axis.[15]

In the $HoBaCo_4O_7$ corner-sharing tetrahedral network, the Co(1)-O(2) and the Co(2)-O(3) bonds are shortened by about

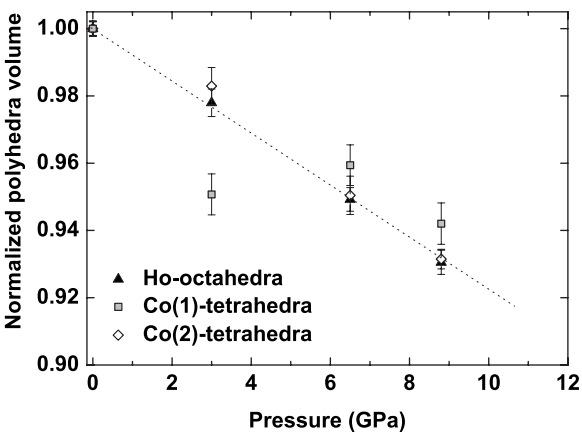

FIG. 8. Normalized HoO_6, $Co(1)O_4$, and $Co(2)O_4$ polyhedron volumes as a function of pressure of $HoBaCo_4O_7$ up to 9 GPa. The dotted line is a guide to the eye.

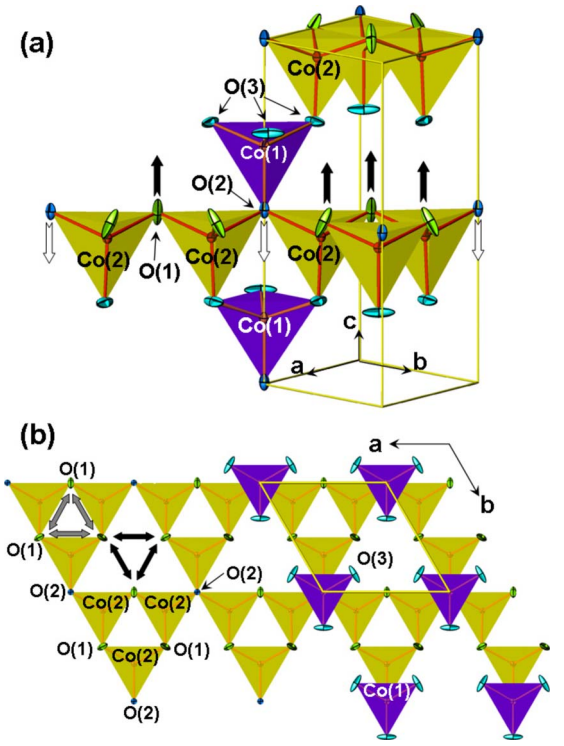

FIG. 9. (Color online) (a) Section of the corner-sharing tetrahedral network, the white and black arrows represent the movement upon pressure. (b) kagomé layer, the gray and black arrows represent the O(1)-O(1) distances of the three-membered and six-membered rings of corner-sharing $Co(2)O_4$ tetrahedra (3-mrt and 6-mrt).

2.6% at 9 GPa, while the Co(2)-O(1), Co(2)-O(2), and Co(1)-O(3) bonds are shortened by 2%, 1.5%, and 1.3%, respectively [Fig. 9(a) and Table IV]. The greater compressibility of the *c* axis is simply a result of the two most compressible bonds being oriented in this direction.

3. Structural compression mechanism of $HoBaCo_4O_7$

Comparing the interatomic distances and the intrapolyhedral angles upon pressure (Table IV and Fig. 10), some changes on the kagomé layers are observed. In order to sketch a model of the structural compression mechanism of $HoBaCo_4O_7$, we will describe the kagomé layers in terms of three-membered and six-membered rings of corner-sharing $Co(2)O_4$ tetrahedra [3-mrt and 6-mrt, Fig. 9(b)]. The effect of pressure is pushing down the O(2) atoms [white arrows Fig. 9(a)]. This decreases the angle Co(1)-O(2)-Co(2) and increases the angle Co(2)-O(2)-Co(2) (Fig. 10). This movement drives the O(1) atoms up [black arrows Fig. 9(a)] increasing the angle O(1)-Co(2)-O(1), decreasing the angle Co(2)-O(1)-Co(2), and decreasing the distance O(1)-O(1) in the three-membered ring polyhedra (Fig. 10). Therefore, the structural compression of $HoBaCo_4O_7$ is mainly achieved by a combination of bond compression and changes in the three-membered and six-membered rings of the kagomé layers.

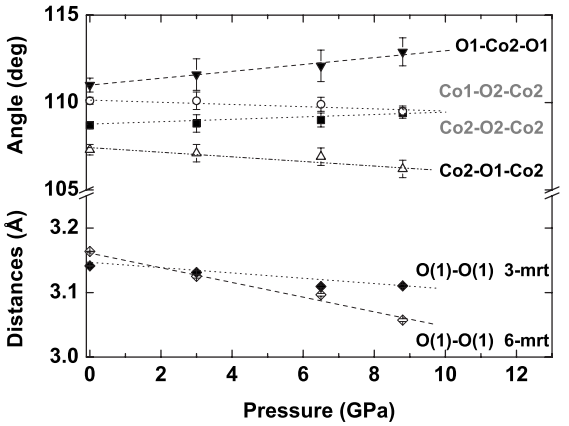

FIG. 10. Intertetrahedra angles of the corner-sharing tetrahedral network and O(1)-O(1) distances of the three-membered and six-membered rings of corner-sharing $Co(2)O_4$ tetrahedra (3-mrt and 6-mrt). The dashed lines are guides to the eye.

IV. CONCLUSIONS

We have shown that the correct space group for $HoBaCo_4O_7$ at ambient conditions is $P6_3mc$. No temperature-induced structural phase transition was detected down to 100 K and no evidence for a pressure-induced structural phase transformation was observed up to 9 GPa. Since phase transitions at low temperature in oxygen nonstoichiometric samples have been reported in several members of the $MBaCo_4O_7$ family, the structural stability of $HoBaCo_4O_7$ could be related to the oxygen stoichiometry of the single crystals used in this study. However, the exact reason for this high structural stability is still open and further experiments using samples with different oxygen content are needed. A fit of a third-order BM-EOS to the *p*-*V* data results in $B_0 = 123(2)$ GPa and $B' = 1.5(2)$. The compressibility of $HoBaCo_4O_7$ is mainly driven by a combination of bond compression and changes in the three-membered and six-membered rings of the kagomé layers. The bonding in the kagomé layers determines the compressibility of these compounds. $HoBaCo_4O_7$ is more compressible than structurally related siliconitrides, aluminiumsiliconoxonitrides, or siliconcarbidenitrides due to the more compressible Co-O bonds. We conclude that the $O^{[4]}$ links play an important role in the oxygen absorption and desorption processes.

ACKNOWLEDGMENTS

The authors gratefully acknowledge financial support from the DFG through research foundation (WI 1232 within the Projects No. SPP-1136 and No. SPP-1236). D.J.W. would like to thank the Materials Grid project for funding. R.B.M. acknowledges the facilities as well as scientific and technical assistance from the staff in the Australian Microscopy and Microanalysis Facility (AMMRF) at the electron microscope unit, The University of Sydney. A.F. thanks the CNV foundation for financial support. E.A.J.A. would like to thank E. Haussühl and L. Bayarjargal (Goethe-Universität Frankfurt) for technical help and D. Argott de Juarez for her comments.

*Present address: CIICAp, The Autonomous University of the State of Morelos, Av. Universidad 1001, Cuernavaca, México. arellano@kristall.uni-frankfurt.de

†Also at Bragg Institute, ANSTO, PMB 1, Menai, NSW 2234, Australia.

[1] D. V. Sheptyakov, A. Podlesnyak, S. N. Barilo, S. V. Shiryaev, G. L. Bychkov, D. D. Khalyavin, D. Y. Chernyshov, and N. I. Leonyuk, in *PSI Scientific Report 2001*, Volume III, Condensed Matter Reseearch with Neutrons, edited by J. Schefer, D. Castellazzi, and M. Shea-Braun, p. 64.

[2] M. Valldor and M. Andersson, Solid State Sci. **4**, 923 (2002).

[3] M. Valldor, Solid State Sci. **6**, 251 (2004).

[4] M. Karppinen, H. Yamauchi, S. Otani, T. Fujita, T. Motohashi, Y. H. Huang, M. Valkeapää, and H. Fjellvag, Chem. Mater. **18**, 490 (2006).

[5] E. V. Tsipis, V. V. Kharton, J. R. Frade, and P. Núñez, J. Solid State Electrochem. **9**, 547 (2005).

[6] A. Huq, J. F. Mitchell, H. Zheng, L. C. Chapon, P. G. Radaelli, K. S. Knight, and P. W. Stephens, J. Solid State Chem. **179**, 1136 (2006).

[7] E. V. Tsipis, D. D. Khalyavin, S. V. Shiryaev, K. S. Redkina, and P. Núñez, Mater. Chem. Phys. **92**, 33 (2005).

[8] E. V. Tsipis, V. V. Kharton, and J. R. Frade, Solid State Ionics **177**, 1823 (2006).

[9] M. Valkeapää, M. Karppinen, T. Motohashi, R.-S. Liu, J.-M. Chen, and H. Yamauchi, Chem. Lett. **36**, 1368 (2007).

[10] O. Chmaissem, H. Zheng, A. Huq, P. W. Stephens, and J. F. Mitchell, J. Solid State Chem. **181**, 664 (2008).

[11] M. Soda, Y. Yasui, M. Taketo, M. Sato, N. Igawa, and K. Kakurai, J. Phys. Soc. Jpn. **75**, 054707 (2006).

[12] L. C. Chapon, P. G. Radaelli, H. Zheng, and J. F. Mitchell, Phys. Rev. B **74**, 172401 (2006).

[13] N. Nakayama, T. Mizota, Y. Ueda, A. N. Sokolov, and A. N. Vasiliev, J. Magn. Magn. Mater. **300**, 98 (2006).

[14] E. A. Juarez-Arellano, A. Friedrich, K. Knorr, A. Lieb, B. Winkler, M. Amboage, M. Hanfland, and W. Schnick, Acta Crystallogr., Sect. B: Struct. Sci. **62**, 424 (2006).

[15] A. Friedrich, K. Knorr, B. Winkler, A. Lieb, H. A. Höppe, W. Schnick, V. Milman, and M. Hanfland, J. Phys. Chem. Solids **70**, 97 (2009).

[16] G. L. Bychkov *et al.*, Cryst. Res. Technol. **40**, 395 (2005).

[17] Oxford Diffraction, CRYSALIS RED, version 171.31.5, Oxford diffraction, Poland, 2006.

[18] M. C. Burla, R. Caliandro, M. Camalli, B. Carrozzini, G. L. Cascarano, L. De Caro, C. Giacovazzo, G. Polidori, and R. Spagna, *SIR-2004. A Program for Automatic Solution and Refinement of Crystal Structure* (C. N. R., Bari, Italy, 2004).

[19] G. M. Sheldrick, Acta Crystallogr., Sect. A: Found. Crystallogr. **64**, 112 (2008).

[20] L. J. Farrugia, J. Appl. Crystallogr. **32**, 837 (1999).

[21] R. Miletich, D. R. Allan, and W. F. Kuhs, *High-Pressure Single-Crystal Techniques*, MSA Reviews in Mineralogy and Geochemistry Vol. 41 (Mineralogical Society of America Reviews in Mineralogy and Geochemistry, Washington D.C., 2000), pp. 445–520.

[22] H. Mao, P. Bell, J. Shaner, and D. Steinberg, J. Appl. Phys. **49**, 3276 (1978).

[23] L. W. Finger and H. E. King, Am. Mineral. **63**, 337 (1978).

[24] K. Eichhorn, REDUCE, HASYLAB/DESY (1987).

[25] K. Eichhorn, AVSORT, HASYLAB/DESY (1978).

[26] R. J. Angel, J. Appl. Crystallogr. **37**, 486 (2004).

[27] R. J. Angel, *EOS-FIT, version 5.2* (Virginia Tech, Blacksburg, U.S.A., 2001).

[28] R. D. Shannon, Acta Crystallogr., Sect. A: Cryst. Phys., Diffr., Theor. Gen. Crystallogr. **32**, 751 (1976).

[29] V. Caignaert, A. Maignan, V. Pralong, S. Hébert, and D. Pelloquin, Solid State Sci. **8**, 1160 (2006).

[30] C. Nather, *Practical Aspects of X-ray Single-Crystal Structure Determination* (Christian-Albrechts-University, Kiel, 2002).

[31] *International Tables for Crystallography*, 5th ed., edited by T. Hahn (The International Union of Crystallography, Kluwer, Dordrecht, Netherlands, 2002), Vol. A.

[32] A. L. Spek, J. Appl. Crystallogr. **36**, 7 (2003).

[33] Y. Le Page, J. Appl. Crystallogr. **20**, 264 (1987).

[34] Y. Le Page, J. Appl. Crystallogr. **21**, 983 (1988).

[35] R. E. Marsh and A. L. Speck, Acta Crystallogr., Sect. B: Struct. Sci. **57**, 800 (2001).

[36] H. Müller-Buschbaum and C. Rabbow, Z. Naturforsch., B: Chem. Sci. **51**, 343 (1996).

[37] M. Valldor, Solid State Sci. **7**, 1163 (2005).

[38] H. Hao, J. Cui, C. Chen, L. Pan, J. Hu, and X. Hu, Solid State Ionics **177**, 631 (2006).

[39] L. Raimondo, M. Laicini, P. Spearman, S. Tavazzi, and A. Borghesi, J. Chem. Phys. **125**, 024702 (2006).

[40] R. J. Angel, *High-Pressure and High-Temperature Crystal Chemistry*, MSA Reviews in Mineralogy and Geochemistry Vol. 41 (Mineralogical Society of America Reviews in Mineralogy and Geochemistry, Washington DC, 2000), pp. 35–60.

[41] A. M. Hofmeister, Geophys. Res. Lett. **20**, 635 (1993).

[42] A. M. Hofmeister and H. K. Mao, Geochim. Cosmochim. Acta **67**, 1215 (2003).

[43] D. Anderson and O. Anderson, J. Geophys. Res. **75**, 3494 (1970).

[44] D. J. Wilson, B. Winkler, E. A. Juarez-Arellano, A. Friedrich, K. Knorr, C. J. Pickard, and V. Milman, J. Phys. Chem. Solids **69**, 1861 (2008).

[45] H. A. Höppe, G. Kotzyba, R. Poettgen, and W. Schnick, J. Mater. Chem. **11**, 3300 (2001).

[46] A. Lieb, J. A. Kechele, R. Kraut, and W. Schnick, Z. Anorg. Allg. Chem. **633**, 166 (2007).

[47] H. Huppertz and W. Schnick, Z. Anorg. Allg. Chem. **623**, 212 (1997).

[48] L. W. Finger, *Volcal* (Carnegie, Washington DC, 1971).